

Gadolinium-doped Cu-In-Zn-S quantum dots: one-pot aqueous synthesis and multimodal bioimaging

L. Zhang^{a,*}, Y. Wan^a, J. Xue^a, W. Duan^a, D. Chen^a, Y. Wu^a, J. Wang^a, D. Xu^a,
D. Liu^b

^aCollege of Medical Technology, Qiqihar Medical University, Qiqihar,
Heilongjiang 161006, China

^bCommunication and Electronic Engineering Institute, Qiqihar University,
Qiqihar, Heilongjiang 161006, China

We report a one-pot method to directly synthesize magnetic resonance/fluorescence multimodal imaging gadolinium-doped Cu-In-Zn-S quantum dots(GCIZS QDs) in aqueous media by using bio-compatible glutathione (GSH) as capping ligand and stabilizer. The optical features and structure of the GCIZS QDs have been characterized by UV-vis and fluorescence spectroscopy, XRD, TEM, and FT-IR. As a result, The GCIZS QDs possessed a strong fluorescence and r_1 value of $4.015 \text{ mM}^{-1}\text{s}^{-1}$ at the Cu/Gd ratio of 1/2. Furthermore, the GCIZS QDs were good water solubility and less cytotoxic up to 250 $\mu\text{g/mL}$ in HUVEC cells. The red emission GCIZS QDs from the MDA-MB-231 cells was clearly observed under microscope. It indicated that the GCIZS QDs present great potential as magnetic resonance /fluorescence multimodal imaging contrast agents for biological labels.

(Received June 22, 2021; Accepted October 7, 2021)

Keywords: GCIZS QDs, gadolinium doped, multimodality imaging, GSH capped

1. Introduction

Multimodal imaging which is synergistically combining several imaging modalities, has been proved to be a powerful tool for early diagnosis and disease treatment with high precision and accuracy. Magnetic resonance(MR)/fluorescence(FL) multimodal imaging has the outstanding advantage of simultaneously offering high-resolution histological information and highly sensitive functional imaging in all multimodal imaging [1,2]. The development of MRI/FL contrast agents has been a hotspot in the fields of materials and medicine. In particular, the research on contrast agents constructed with gadoliniumchelates and semiconductor quantum dots (QDs) has attracted considerable attention. On account of its characteristic of accelerating the longitudinal relaxation rate (r_1), gadolinium exhibits bright contrast, which with its lowered cytotoxicity has been widely used clinically after coordination to a polydentate chelator, e.g., DTPA and DTTA. Semiconductor QDs have distinguished emission profiles such as composition and size dependent absorption and emission, and a long fluorescence lifetime[3,4]. Relevant studies have been focused on II–VI or IV–VI QDs such as CdSe, CdTe and PbTe which have high quantum yields and relatively strong photoluminescence emission. Unfortunately, the toxicity of the Cd/Pb-based QDs limits their

* Corresponding author: zhangliping1978@163.com

applications in the biological field[4,5]. Although various protections employing polymers, ZnS, and other nontoxic shells have been developed, the leakage of Cd/Pb ions through the shell and the radicals derived from light irradiation could still be observed [6,7].

Consequently, heavy-metal-free QDs have been gaining increased attention[8]. For example, copper chalcogenide based QDs have recently been extensively investigated due to their low toxicity(e.g. CuInS₂, CuInZnS)[9,10]. There are many limitations about the existing synthesis of CIZS QDs. Firstly, most reports about quaternary CIZS QDs have been synthesized in complicated organometallic procedure with high reaction temperature and low efficiency[11-14]. Secondly, the as-prepared hydrophobic QDs in organic phase are poor biocompatibility and high biotoxicity. The indispensable ligand exchange and surface modification are required for hydrophobic QDs can result in degradation of QDs photoluminescence performance. Therefore, it is necessary to develop a novel synthesis method to obtain hydrophilic and high quality CIZS QDs without any organometallic or toxic precursors.

In order to the above problems, We report a one-pot method to directly synthesize magnetic resonance/fluorescence multimodal imaging GCIZS QDs. Compared with previous reports, our strategy only utilized GSH as the stabilizer and capping ligand. GSH capped QDs were considered more biocompatible as compared to other thiol capping ligands[15, 16]. The prepared GCIZS QDs were highly biocompatible and showed bright red fluorescence bioimaging of MDA-MB-231 cells.

2. Experimental details

2.1. Chemicals

CuCl₂·2H₂O(AR), InCl₃·4H₂O(98%), Zn(AC)₂·2H₂O(99.0%), GdCl₃·6H₂O(99.9%), DTPA(99%), C₂H₅NS (≥98.0%), and GSH(98%) were purchased from Aladdin Inc. NaOH was purchased from Macklin Inc. ethanol absolute(99.7%) and N-hexane(97.0%) were purchased from Sinopharm Chemical Reagent Co., Ltd.

2.2. Synthesis of GCIZS QDs

GCIZS QDs were synthesized in aqueous solution via a hydrothermal synthesis method. In a typical experiment, GdCl₃·6H₂O(0.025 mmol) and DTPA(0.075 mmol) were dissolved in deionized water (17 mL) by vigorous stirring at 50°C for 30 minutes. After naturally cooling to room temperature, CuCl₂·2H₂O(0.0125 mmol), InCl₃·4H₂O(0.125 mmol), Zn(AC)₂·2H₂O(0.0625 mmol), and GSH (0.875 mmol) was injected into the solution. The pH value of the mixture solution was adjusted to 11 by adding 2.0 mol·L⁻¹ NaOH solution with stirring. During this process, the solution changed from turbid to clear. In the meantime, C₂H₅NS (0.875 mmol) was dissolved 3 mL deionized water. After ultrasound for 10 minutes, C₂H₅NS was rapidly injected into the prior mixed solution. After vigorous stirring for 6 minutes, the solution was transferred into a Taflon-lined stainless steel autoclave with a volume of 25 mL. The autoclave was maintained at 120°C for 4h and then cooled down to room temperature by a natural cooling process. The GCIZS QDs powder could be precipitated by ethanol absolute, and the precipitate was isolated by centrifugation, washed with ethanol absolute and N-hexane several times, then GCIZS QDs were obtained.

2.3. Cytotoxicity and cellular imaging

MTT assay was employed to evaluate the cytotoxicity of the as-prepared GCIZS QDs using HUVEC cells. In brief, HUVEC cells were seeded on a 96-well plate at an initial density of 3×10^4 cells per well and incubated. After incubation for 24 h, the cells were washed with PBS for three times and 20 μL of MTT solution (dissolved in PBS, $5 \text{ mg} \cdot \text{mL}^{-1}$) were added to each well, followed by incubation for another 4 h. All the incubation process stated above were performed at 37°C with 5% CO_2 . Finally, the supernatant was removed and 150 μL of DMSO was added to each well. At last absorption at 570 nm was measured by using plate reader.

2.4. Cellular imaging

The ability and facility of the synthesized GCIZS QDs for cellular imaging were evaluated by the fluorescence imaging of MDA-MB-231 cells. MDA-MB-231 cells were seeded in a 24-well plate at 37°C for 24 h. The concentration of GCIZS QDs solution for cellular imaging was $0.0625 \text{ mg} \cdot \text{mL}^{-1}$. The cells were treated with the GCIZS QDs solution for another 24 h, followed by washed with PBS for three times. The fluorescence images were acquired by a fluorescent microscope.

2.5. Characterization

XRD data were obtained on a Bruker D8 Advance X-ray diffractometer using Cu-K α irradiation at $\lambda = 0.15418 \text{ nm}$. TEM images were recorded on a Hitachi H-7650 electron instrument. FTIR spectra were recorded in $400 \sim 4000 \text{ cm}^{-1}$ on a Nicolet 380 spectrophotometer using a KBr pellet. UV-Vis absorption spectra were obtained using a Shimadzu UV-2550 spectrometer. Photoluminescence measurements were carried out at room temperature with a Shimadzu RF-5301PC spectrofluorometer. The fluorescence imaging of cells were observed using Olympus-IX73-DP80 inverted fluorescence microscope.

3. Results and discussion

3.1. Structural characterization

Fig. 1(a) showed the XRD patterns of CIZS QDs and GCIZS QDs. From the curve, three main peaks around 27.7° , 47.3° , and 55.5° can be observed, corresponding to the (002), (110), and (112) phases of hexagonal structure, respectively. The broad diffraction peaks could be explained by the small size of the nanoparticle. On the other hand, no diffraction peak belonging to a new phase of free Gd ions is found in the XRD patterns of GCIZS QDs, indicating that the Gd is stably coordinated with CIZS QDs.

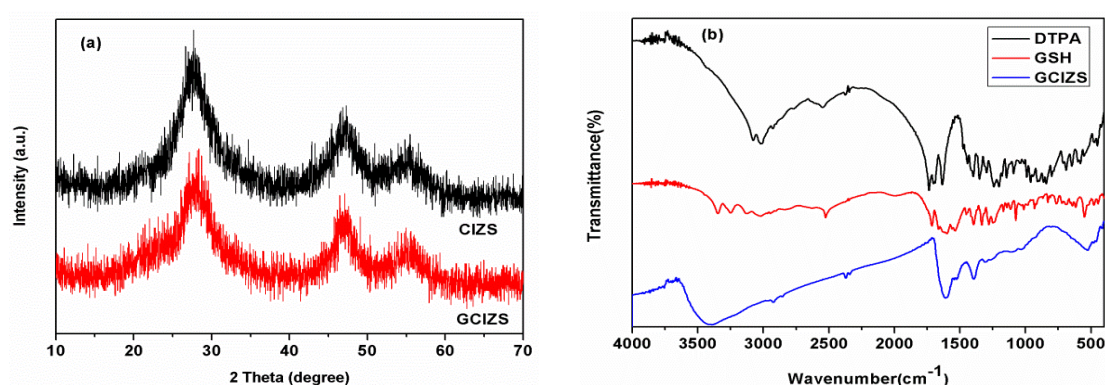


Fig. 1. (a) XRD patterns of CIZS QDs (top) and GCIZS QDs (bottom) (b) FT-IR spectra of pure DTPA (top), GSH (middle) and GCIZS QDs (bottom).

The FT-IR spectra of GSH, DTPA and GCIZS QDs synthesized at 120 °C for 4 h with the Cu/In molar ratio of 1:10 are shown in Fig. 1(b). The peaks located at 3022 cm^{-1} , 3249 cm^{-1} , 3346 cm^{-1} and 3126 cm^{-1} of GSH were attributed to the N-H and C-O stretching vibration. The disappearance of the two peaks at 2525 cm^{-1} and 1536 cm^{-1} , ascribed to the -SH stretching vibration and -NHR deformation vibration, indicating that the GSH was combined into the surface of GCIZS QDs. In addition, The DTPA spectrum showed shoulder peaks at 1703 cm^{-1} and 1733 cm^{-1} for the stretching vibration band due to the C=O in the free carboxy group. After the reaction, this characteristic band disappeared while the characteristic band assigned to the -COO⁻ group at around 1613 cm^{-1} appeared, which indicated that the free carboxyl groups in the DTPA had chelated with Gd by deprotonation.

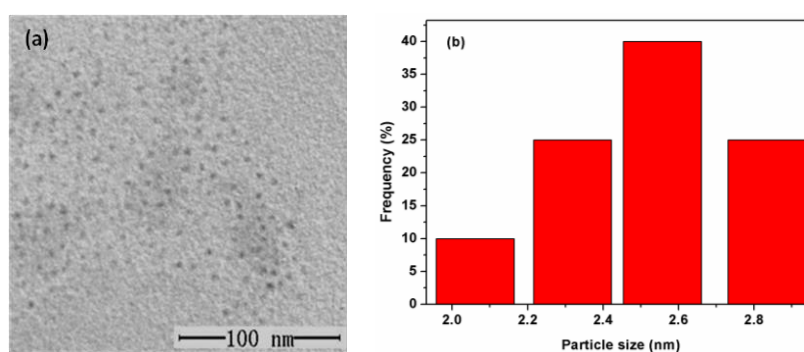


Fig. 2. TEM images (a) and size distribution (b) of GCIZS QDs under optimum experimental conditions.

Fig.2 (a) showed the TEM images of GCIZS QDs prepared under optimum experimental conditions. It is obvious that GCIZS QDs are near-spherical shape and well-dispersed. Fig.2 (b) displayed size distribution histograms of CIZS QDs and the mean particle size was 2.55 nm. The size distribution histograms were obtained from the TEM images.

3.2. Optical Properties of the GCIZS QDs

Fig. 3 showed the absorption spectra(a) and PL spectra(b) of GCIZS QDs with different Cu/Gd molar ratios. It showed that the absorption edge of UV-Vis absorption spectrum and the peak of fluorescence spectrum are red shifted with the molar ratio of Cu/Gd varying from 1:0 to 1:5. This indicated that the particle size of GCIZS QDs increased slightly with the increased of Gd content. This is likely because the ionic radius of Gd^{3+} (0.094 nm) is larger than that of Cu^+ (0.077 nm), Zn^{2+} (0.074 nm), and In^{3+} (0.080 nm), thus the radius of GCIZS QDs increased accordingly with the increase of Gd doping.

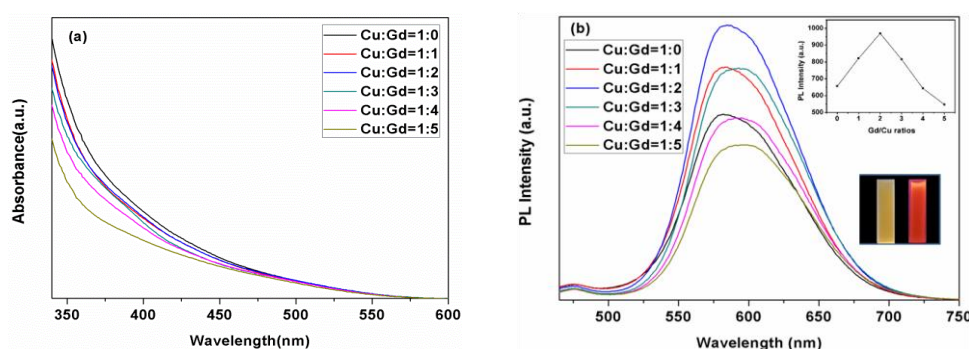


Fig. 3. The absorption spectra(a) and PL spectra(b) of GCIZS QDs with different Cu/Gd molar ratios.

Fig. 3(b) showed the PL intensity reached a maximum value at Cu/Gd = 1:2. This is likely because GCIZS QDs exhibit a defect-dependent PL emission related to copper deficiency, the existence of defect pairs of copper vacancies and other cations on Cu antisite contributes to the PL emission of GCIZS QDs following a donor acceptor pair recombination mechanism. The introduction of Gd species creates more defects thus can potentially increase fluorescence, whereas the paramagnetic Gd species could also compromise the PL emission. Therefore, the competitive balance was achieved at the molar ratio of Cu/Gd = 1:2, resulting optimized PL intensity. The inset in Fig.3(b) shown the digital camera of the GCIZS QDs, from which it could be seen that the GCIZS QDs emit strong orange fluorescence under the irradiation of 365 nm UV lamp and is yellow under daylight irradiation.

3.3. Magnetic Properties of GCIZS QDs

To evaluate the ability of GCIZS QDs as an effective MR contrast agent, the longitudinal (T_1) and transverse (T_2) proton relaxation times were measured. As summarized in Fig. 4(a), the GCIZS QDs exhibited r_1 value of $4.015 \text{ mM}^{-1}\text{s}^{-1}$. It has been demonstrated that the relaxivity ratio (r_2/r_1) is a crucial parameter to evaluate the efficiency of T_1 contrast agents, that is, low r_2/r_1 ratio less than 3.0 tends to produce a desired T_1 contrast effect. In this study, the GCIZS QDs possessed a relatively low r_2/r_1 ratio of 1.98, suggested that the GCIZS QDs were efficient T_1 contrast agents.

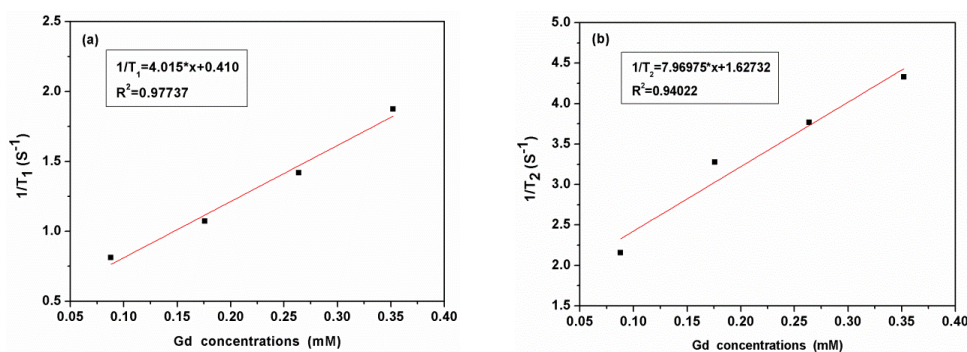


Fig. 4. Magnetic Properties of GCIZS QDs: (a) Longitudinal rates ($1/T_1$, s⁻¹), (b) transverse rates ($1/T_2$, s⁻¹).

3.4. Biocompatibility of GCIZS QDs

In vitro cytotoxicity of the GCIZS QDs against HUVEC cells following 24 h, 48 h, and 72 h. The cytotoxicity of GCIZS QDs was evaluated via MTT assay by incubating HUVEC cells with GCIZS QDs at various concentrations of Gd, respectively. The MTT results in Fig. 5 indicated that the GCIZS QDs showed little cytotoxicity against HUVEC cells even at Gd concentrations up to 0.25 mM, confirming good biocompatibility of GCIZS QDs towards HUVEC cells and emphasizing its potential applications in bioimaging.

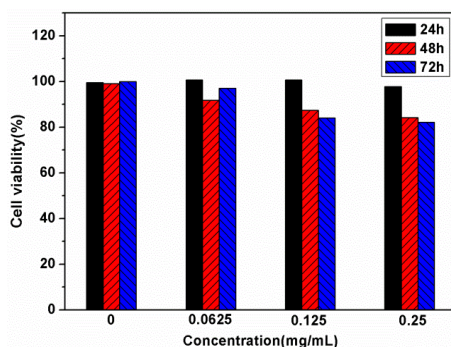


Fig. 5. Viabilities of cells incubated with different concentration of GCIZS QDs.

3.5. Cell labeling

Fig.6 showed the fluorescent image of MDA-MB-231 cells incubated with GCIZS QDs. The red emission GCIZS QDs from the cells was clearly observed under fluorescent microscope, which suggested that GCIZS QDs can successfully enter into the MDA-MB-231 cells. This phenomenon showed that the GCIZS QDs can perform as biomarkers for cancer cell fluorescence imaging. Compared with cadmium containing QDs, the toxicity of GCIZS QDs was much less and therefore had more advantages for future clinical applications.

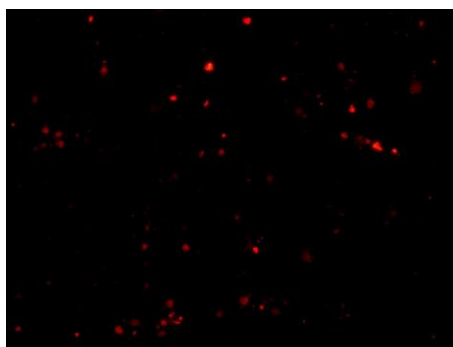


Fig. 6. The fluorescent image of MDA-MB-231 cells labeled.

4. Conclusions

In summary, a facile one-pot method to directly synthesize magnetic resonance/fluorescence multimodal imaging GCIZS QDs in aqueous media by using bio-compatible glutathione (GSH) as capping ligand and stabilizer. As a result, The GCIZS QDs possessed a strong fluorescence and r_1 value of $4.015 \text{ mM}^{-1}\text{s}^{-1}$ at the Cu/Gd ratio of 1/2. Furthermore, the GCIZS QDs were good water solubility and less cytotoxic up to $250 \mu\text{g/mL}$ in HUVEC cells. At the same time, the red emission GCIZS QDs from the cells was clearly observed under fluorescent microscope, which suggested that GCIZS QDs can successfully enter into the MDA-MB-231 cells. It indicated that the GCIZS QDs present great potential as magnetic resonance /fluorescence multimodal imaging contrast agents for biological labels.

Acknowledgments

This work was financially supported by the Scientific Research Foundation from Education Department of Heilongjiang Province (No. 2018-KYYWF-0086).

References

- [1] H. Yang, S. Santra, G. A. Walter, P. H. Holloway, *Advanced Materials* **18**, 2890 (2006).
- [2] E. S. Shibu, K. Ono, S. Sugino, A. Nishioka, A. Yasuda, Y. Shigeri, S. Wakida, M. Sawada, V. Biju, *Nano* **7**, 9851 (2013).
- [3] L. Jing, K. Ding, S. V. Kershaw, I. M. Kempson, A. L. Rogach, M. Gao, *Advanced Materials* **26**, 6367 (2014).
- [4] A. M. Derfus, W. C. W. Chan, S. N. Bhatia, *Nano Letters* **4**, 11 (2003).
- [5] L. Lai, J. C. Jin, Z. Q. Xu, Y. S. Ge, F. L. Jiang, Y. Liu, *Journal of Membrane Biology* **248**, 727 (2015).
- [6] L. J. Zhang, H. F. Yu, W. Cao, C. Zou, *Micro & Nano Letters* **9**, 55 (2014).
- [7] Y. W. Lan, K. Yang, Y. L. Wang, H. Li, *Micro & Nano Letters* **9**, 202 (2014).
- [8] D. W. Deng, L. Z. Qu, J. Zhang, Y. X. Ma, Y. Q. Gu, *Appl. Mater. Interfaces* **5**,

- 10858 (2013).
- [9] D. Aldakov, A. Lefrancois, P. Reiss, *J. Mater. Chem. C* **1**, 3756 (2013).
- [10] O. Yarema, D. Bozyigit, I. Rousseau, L. Nowack, M. Yarema, W. Heiss, V. Wood, *Chem Mater.* **25**, 3753 (2013).
- [11] W. D. Xiang, X. Ma, L. Luo, W. Cai, C. P. Xie, X. J. Liang, *Mater. Chem. Phys.* **149-150**, 437 (2015).
- [12] L. W. Liu, R. Hu, W. C. Law, I. Roy, J. Zhu, L. Ye, S. Y. Hu, X. H. Zhang, K. T. Yong, *Analyst* **138**, 6144 (2013).
- [13] W. Y. Liu, Y. Zhang, W. W. Zhai, Y. H. Wang, T. Q. Zhang, P. F. Gu, H. R. Chu, H. Z. Zhang, T. Cui, Y. D. Wang, J. Zhao, *J. Phys. Chem. C* **117**, 19288 (2013).
- [14] W. J. Zhang, X. H. Zhong, *Inorg. Chem.* **50**, 4065 (2011).
- [15] L. Ding, P. J. Zhou, H. Zhan, C. Chen, W. Hu, T. F. Zhou, C. W. Lin, *Journal of Luminescence* **142**, 167 (2013).
- [16] Y. Zheng, S. Gao, J. Y. Ying, *Adv. Mater.* **19**, 376 (2007).